

SYSTEMATIC STUDY OF THE ROUGHNESS OF BIODEGRADABLE POLYMER SURFACES PROCESSED BY ULTRASHORT LASER PULSES

Paper Number (#1004)

Bernhard Fäßler¹, Giovanni Piredda¹ and Johann Zehetner¹

¹ Josef-Ressel-Center for material processing with ultra-short pulsed lasers, Research Center for Microtechnology, Vorarlberg University of Applied Sciences, Hochschulstraße 1, 6850 Dornbirn, Austria

Abstract

Polymer-based materials are increasingly common in medical fields, ranging from simple disposable products to complex implants. Polymers have a large variety of physical and chemical properties, fit for use in different medical applications; in particular, biodegradable polymers are interesting for the use as temporary implants - for example in the case of stents, where, after the support phase of a hollow organ the stent can be decomposed by the human body. Roughness of the polymer surfaces is an important parameter for applications. For example, it influences strongly the clinical outcome of stents treatments [1]; as another example, an appropriate surface quality provides a good breeding ground for cell growth [2]. Therefore, precise control over this parameter is desirable. Surface roughness achieved using ultrashort-pulse laser machining depends on processing conditions. The goal of this paper is a systematic investigation of the surface roughness of laser-ablated surfaces as a function of laser processing parameters. To this purpose we machined an array of squares on a sheet of poly(Lactic acid) (PLA) using laser pulses of 350 fs duration at the wavelength of 518 nm. We varied systematically across the array the pulse-to-pulse translation distance, the repetition frequency and the fluence of the laser pulses. We measured the topography of the machined surfaces with a scanning confocal microscope; from the measured surface topography we calculated the standard roughness parameters (arithmetic average) and (root mean square average) [3], obtaining in this way a map of roughness as a function of processing parameters. This map can be used to select appropriate processing parameters for machining surfaces with desired roughness characteristics.

Introduction

Polymer-based materials are increasingly common in medical fields, ranging from simple disposable products to complex implants. Polymers have a large variety of physical and chemical properties, fit for use in different medical applications; in particular, biodegradable polymers are interesting for the use as

temporary implants - for example in the case of stents, where, after the support phase of a hollow organ the stent can be decomposed by the human body. Roughness of the polymer surfaces is an important parameter for applications. For example, it influences strongly the clinical outcome of stents treatments [1]; as another example, an appropriate surface quality provides a good breeding ground for cell growth [2]. Therefore, precise control over this parameter is desirable. Surface roughness achieved using ultrashort-pulse laser machining depends on processing conditions. Laser machining makes it possible to manufacture microstructures with high accuracy and relatively low cost. For medical use it is essential that the fabricated devices are free of harmful substances. Continuous-wave and long-pulse lasers generate high temperatures during the manufacturing process; as a consequence polymers can degrade and harmful substances can be generated. Femtosecond lasers enable the so-called cold ablation and thermal degradation is largely avoided. In addition structural distortions around the ablation area are significantly reduced, which is essential for the performance of microstructures [4].

In this paper we perform a systematic study of the surface roughness of laser-ablated surfaces as a function of laser processing parameters. After a description of the experimental procedure we analyze the texture and roughness of the machined surface resulting from the experiments in three different steps: a qualitative examination at the optical microscope, ablation depth measurement and topography measurement with the help of a scanning confocal microscope. The topography measurements allow us to extract the standard roughness parameters (arithmetic average) and (root mean square average) [3]; we can then discuss the dependence of the roughness parameters from the machining conditions and the possibility of independent selection of ablation depth and surface roughness.

Experimental setup

For our experiments poly (Lactic acid) (PLA) is used. PLA is a biodegradable polymer derived from lactic

acid, a material which can be obtained from renewable resources; it has a wide array of medical applications [4]. For our experiments we used 200 μm -thick PLA sheets (courtesy of BJE Kunststoffe, Diepoldsau, Switzerland) of molar mass-average is 139 g/mol and molar number-average is 69 g/mol (both measured by gel permeation chromatography at the Fraunhofer Institute for Applied Polymer Research in Potsdam-Golm, Germany); the polymer sheets are not of medical grade.

We machined an array of square pockets on a PLA sheet using laser pulses of 350 fs duration at the wavelength of 518 nm. We varied systematically across the array the pulse-to-pulse translation distance, the repetition frequency and the fluence of the laser pulses. After a qualitative evaluation of the surface texture, we measured the depth of the ablated pockets using an optical microscope and the topography of the machined pockets surfaces with a scanning confocal microscope (NanoFocus; μSurf); from the measured surface topography we calculated the standard roughness parameters (arithmetic average) and (root mean square average) [3], obtaining in this way a map of roughness as a function of processing parameters. This map can be used to select appropriate processing parameters for machining surfaces with desired roughness characteristics. We performed both single- and multi-pass experiments; in multi-pass experiments we machined a surface several times with the same laser parameters.

As a light source we use the regenerative amplifier HighQ Spirit (High Q Laser GmbH) emitting pulses of 350 fs duration at a wavelength of 518 nm. The measured spot size of the laser beam waist is $w = 9.4 \mu\text{m}$.

We machine the surface scanning the focused laser beam line by line; the scanning mirrors (intelliScan, Scanlab) are integrated together with the laser, the focusing optics and the vacuum chuck on which the sample is placed in a machining center (microSTRUCT vario, 3D-Micromac); the focusing on the surface is realized by means of the optical measuring device Keyence LK-G152, also integrated in the machining center.

To arrange the systematic study in a practical way, the array of machined square pockets is organized into matrices. All of the pockets of a given matrix are machined with the same pulse energy; different pockets of a given matrix are machined with varying pulse-to-pulse translation distance and laser repetition frequency. Figure 1 shows the layout of a matrix of

pockets for a single-pass experiment and indicates the way in which machining parameters are varied.

Table 1: Machining parameters

Pulse energy [W] (measured at 200 kHz)					
100%	75%	50%	25%	12.5%	6.25%
1.601	1.147	0.68	0.24	0.072	0.016
Pulse-to-pulse translation distance [μm]					
10	8	6	4	2	1
Repetition frequency [kHz]					
100	50	33.33	25	12.5	6.25

Each matrix consists of several pockets which have a size of 1 mm x 1 mm; each pocket consists of many parallel individual laser-machined lines; the machining strategy is unidirectional: each single line is machined in the same direction, from left to right.

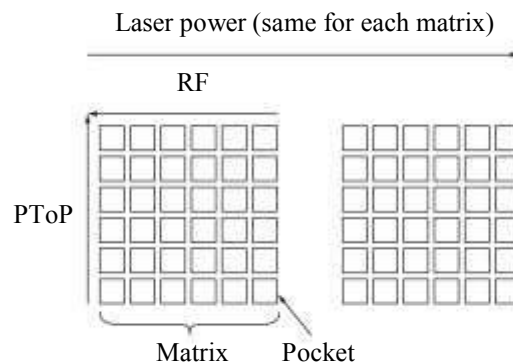


Figure 1: Layout of the pocket array for an ablation experiment. PToP is the pulse-to-pulse translation distance and RF is the laser repetition frequency. Machining parameters increase for each matrix along the direction of the arrows and are the same for corresponding pockets of different matrices; different matrices are machined with different pulse energies.

The pulse-to-pulse translation distance (PToP) is the distance between two subsequent laser pulses along a machining line; to ensure a continuous surface treatment this distance cannot be much larger than the beam waist diameter ($w = 9.4 \mu\text{m}$), otherwise there is no overlap of the individual pulses. We set the distance between parallel lines to be equal to the translation distance between individual pulses along a single line. The regenerative amplifier emits pulses at the base repetition frequency of 200 kHz; through the use of a pulse picker we reach lower repetition frequencies (RF).

In each matrix the pulse-to-pulse translation distance and the repetition frequency are changed along respectively columns and rows. The pulse-to-pulse translation distance is the same along rows; in this way each pocket belonging to a given row is machined with the same number of laser pulses, and is consequently irradiated with the same energy (for a given matrix: the pulse energy changes for different matrices). Along each column the laser repetition frequency is kept constant and the pulse-to-pulse translation distance is varied so that a different amount of laser pulses are used in each pocket, increasing from the top to the bottom of each matrix. We don't use assistant gas during the machining. Table 1 lists the parameters we used for the single-pass experiment; the set of all pockets contained in six matrices (each corresponding to one of the power levels given in Table 1) realizes all possible combinations of the listed parameters.

All the machining programs are written in Visual Basic Script. They can be interpreted, simulated and executed by the control software microMMI and carried out in the microSTRUCT vario machining center.

Figure 2 shows an array of six matrices machined with the parameter set of Table 1. Only four matrices (1-4) are clearly visible; the pockets of matrices five and six are machined close to or below the ablation threshold, therefore they are not or are only faintly visible. The black mark, which can be observed between matrix 2 and 5, is used by the Keyence measuring device to measure the distance to the otherwise transparent surface. Each pocket is machined by one pass of the laser.

The single-pass experiment is extended for five selected pockets with additional passes. The layout of a multi-pass experiment is shown in Figure 3. The machining parameters (pulse energy, repetition rate and pulse-to-pulse translation distance) are kept fixed along rows. All the pockets of the first column are machined by one pass; the pockets of the second column are machined twice and so on until five machining passes are applied to the pockets of the last column.

The parameters used for each row of the multi-pass machining experiment are listed in Table 2.

We cleaned the samples before and after the machining in an ultrasonic bath filled with a solution of 5 ml isopropanol in 100 ml deionized water for 10 minutes (with a recipe that has been demonstrated as effective and safe in [5]); after the cleaning an examination with the optical microscope shows that the surface is free of machining debris.

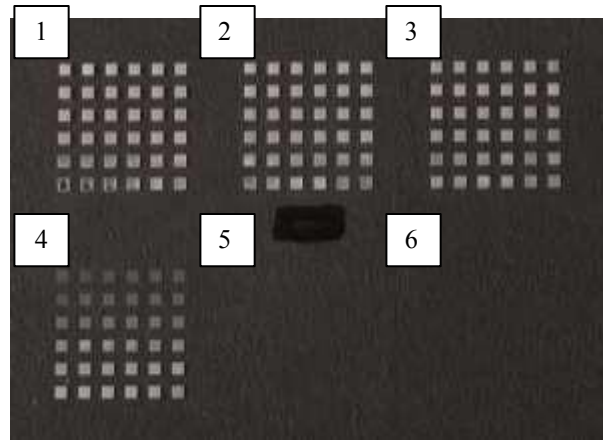


Figure 2: Set of six matrices machined with a single pass of the laser; the machining parameters are given in Table 1.



Figure 3: Matrix of pockets machined with multiple passes of the laser. In each row the machining parameters are held fixed and the number of passes increases from left to right.

Table 2: Machining parameters for each row of the multi-pass experiment measured at 200 kHz

		Parameters (constant along each row)		
		Pulse energy (W)	PToP (μm)	RF (kHz)
Row	1	1.601	4	25
	2	1.147	6	33.3
	3	1.147	8	12.5
	4	0.68	2	12.5
	5	0.24	1	6.25

The machined pockets are analyzed first with a qualitative examination with the optical microscope, followed by depth measurement and topography measurement. Subsequently, the topography data are processed with the help of the software Matlab version R2010a. In order to increase the reflection from the pockets and therefore improve the quality of the confocal microscope measurements we sputter-coated the sample with a 10 nm thick titanium layer; the roughness of the machined surfaces is in the μm range,

therefore a coating of thickness in the few-nm range has no significant effect on the topography measurement.

Optical microscope examination

For the qualitative examination of the ablated pockets we use an optical microscope (Olympus Measuring Microscope stm-um). We use an objective with 50x magnification and a numerical aperture of 0.7. We examined both uncleaned and uncoated pockets (as obtained immediately after machining) and cleaned and coated pockets (which are also used for further investigations); the uncleaned and uncoated pockets are more suited to detect thermal effects of the machining on the samples. We classify the pockets into four categories according to their surface texture in the uncleaned and uncoated state:

- no debris,
- debris,
- melted,
- no ablation

We discuss our classification in the following paragraphs.

No debris

No debris means that no ablated material barely attached to the surface is present; an example for the “no debris” case is shown in Figure 4. This kind of surface texture appears in all power classes for which ablation takes place (100%, 75%, 50% and 25% pulse energy; the corresponding values of the power are listed in Table 1) for large pulse-to-pulse translation distances (10 μm – 4 μm) and middle-to-high repetition frequencies (100 kHz – 25 kHz).

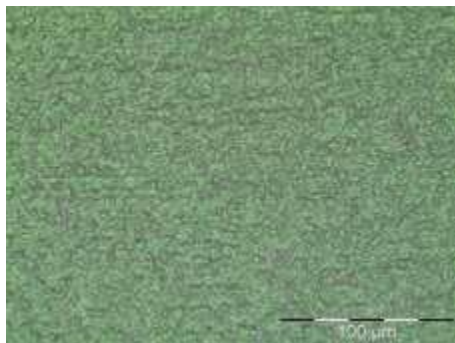


Figure 4: Example of a machined surface without debris

Debris

Debris means ablated material which is loosely connected to the surface. The debris generated by our machining process looks under the microscope like

melted or evaporated material which has resolidified; it can be removed by light scratching with tweezers. An example of debris can be seen in Figure 5. “Debris” cases occur in all power classes for small pulse-to-pulse translation distances (4 μm – 1 μm) and mostly low repetition frequencies; there is a smooth transition between “debris” and “no debris” and the classification of the transition cases is subjective.

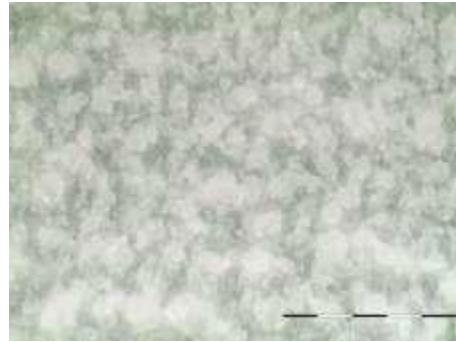


Figure 5: Example of a machined surface with debris

Melted

In the case of melting the surface is melted and resolidified. The occurrence of whole-surface melting is visible in higher power classes (100% and 75% pulse energy) for small pulse-to-pulse translation distances (2 μm – 1 μm) and higher repetition frequencies (100 kHz – 33.33 kHz). An example of a melted surface texture can be seen in Figure 6.

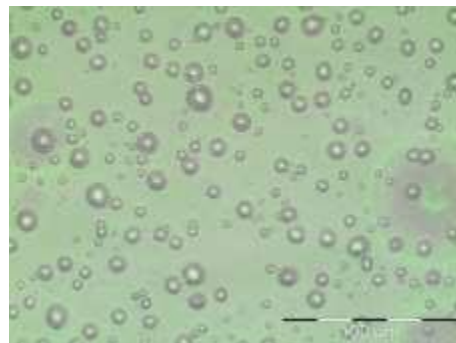


Figure 6: Example of a melted surface

No ablation

There are some pockets where no ablation occurs. This happens predominantly at low pulse energies (12.5% and 6.25%; the corresponding values of the power are listed in Table 1), as in this case the laser fluence is below the ablation threshold damage.

We classify in Table 3 the pockets belonging to four of the six single-pass matrices we machined according to the four categories we described. The four classified matrices are the ones machined with pulse energy

equal to 100%, 75%, 50%, and 25% (corresponding values of the power in Table 1). In none of the pockets of matrices five and six are ablation occurs; the laser fluence is below the ablation threshold. Green marked areas correspond to surfaces without debris, blue ones with debris; red color indicates melted surfaces and white indicates surfaces where no significant ablation occurred. Also two pockets completely burned through in Matrix 1.

Table 3: Classification of the ablated pockets according to their surface texture (see the text for a description of the categories)

		RF [kHz]											
		100	50	33.33	25	12.50	6.25						
Pulse energy = 100 %													
PToP (μm)	10	no debris					debris						
	8												
	6												
	4												
	2	melted		debris									
	1	burned through											
Pulse energy = 75 %													
PToP (μm)	10	no debris					debris						
	8												
	6												
	4												
	2	melted		debris									
	1	melted											
Pulse energy = 50 %													
PToP (μm)	10	no debris					debris						
	8												
	6												
	4												
	2	melted		debris									
	1	melted											
Pulse energy = 25 %													
PToP (μm)	10	No ablation											
	8												
	6												
	4												
	2							debris					
	1												

Surface topography analysis part 1: depth and ablation rate

Keeping in mind the surface texture classification we take a closer look at the machined surfaces, examining more closely in the next two steps the connection between the surface texture, the depth and the machining parameters; additionally we calculate the ablation rate.

We measure the depth of each pocket with the same microscope we used for the qualitative surface texture examination (Olympus Measuring Microscope stmum) and the same objective (50x magnification, 0.7 numerical aperture); the resolution in all axes of the measuring system is about 500 nm. The depth measurement is realized by focusing in sequence on the bottom of the ablated pocket and on the top surface of the un-ablated polymer sheet and reading the difference in height between the two points on microscope measuring system. Once collected, the depth values belonging to one matrix, machined with specific pulse energy, are plotted against the pulse-to-pulse translation distance and the repetition frequency; in Figure 7, as an example, we plot the depth values for 100% pulse energy.

In order to make a possible trend of depth against the pulse-to-pulse translation distance and the repetition frequency visible, a fit function is placed through the data points.

The fitting function is developed according to the following consideration; the amount of ablated material should increase with the energy that is absorbed by the sample; this is in turn, in our experiments, proportional to the inverse of the square of pulse-to-pulse translation distance.

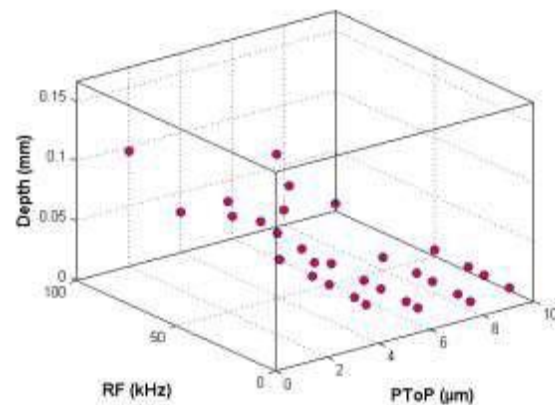


Figure 7: Depth of the pockets machined with 100% pulse energy plotted against pulse-to-pulse translation distance (μm) and repetition frequency (kHz)

Based on this idea we tried as a reasonable fit function an inverse polynomial in pulse-to-pulse translation distance:

$$D = \frac{a}{PToP^b} + c \quad (1)$$

Here, a , b and c are coefficients of the fit function, which are determined according to the least-squares criterion; for the determination of the fit coefficients we use the fitting routine `fitype` of the Fitting Toolbox of Matlab version R2010a. The best-fitting function can be seen in Figure 8; the fit is excellent; the presence of an excellent fitting function gives the possibility to predict the depth of a pocket machined with a given set of laser parameters.

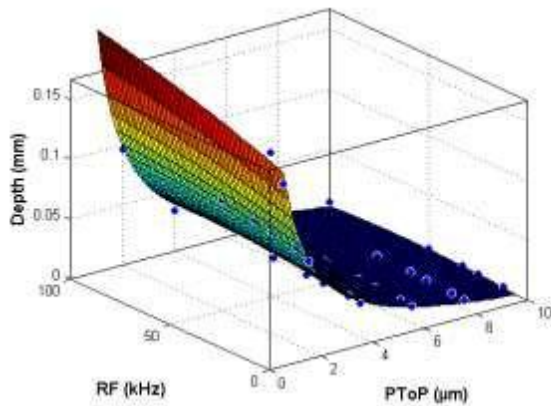


Figure 8: Depth of the pockets machined with 100% pulse energy plotted against pulse-to-pulse translation distance (μm) and repetition frequency (kHz) and corresponding best-fitting function

Using the depth data and the machining parameters the ablation rate (ablated volume per unit time) for each individual pocket can be calculated according to the following equation:

$$AR = \frac{D}{t} \quad (2)$$

The laser path length is the length of the path along which the laser beam is scanned to machine the given pocket while the product of the pulse to pulse translation distance and the laser repetition frequency gives the speed at which the scanned beam moves on the surface.

The fitting function for the ablation rate can be then derived directly from the fitting function used for the depth as:

$$AR = \frac{a}{PToP^b} + c \quad (3)$$

The fit function coefficients are the same coefficients obtained for the depth fit; Figure 9 shows the fitted function through the ablation rate data points for 100% pulse energy.

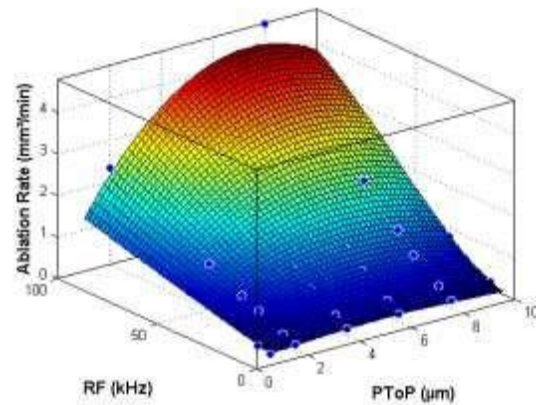


Figure 9: Ablation rate of the pockets machined with 100% pulse energy plotted against pulse-to-pulse translation distance (μm) and repetition frequency (kHz) and corresponding best-fitting function

Surface topography analysis part 2: roughness

In the third analysis step the surface roughness is examined. The surface topography of the machined pockets belonging to matrices 1 to 4 is measured with the confocal microscope. The raw surface topography data are analyzed with the help of Matlab version R2010a.

The analysis consists in the following steps. First, the topography of given pocket is filtered to separate it into waviness, roughness and noise components. We use for this purpose Fourier filters which split the surface topography data in low, middle and high frequency components; the low-pass filter selects the waviness and the high-pass filter selects the noise; what remains after subtracting waviness and noise is the roughness. Subsequently the roughness values and R_a for each single pocket are calculated according to the following equations:

$$R_a = \frac{1}{A} \iint_A |z(x,y) - \bar{z}| dx dy \quad (4)$$

$$\sqrt{\frac{1}{A} \iint_A (z(x,y) - \bar{z})^2 dx dy} \quad (5)$$

The arithmetic average S_a describes the average of the absolute values of the deviations from the nominal surface over a given measurement area [6]. The root mean square average S_q corresponds to the square root of the average of the square of the profile deviation. It is more sensitive to individual peaks than the arithmetic mean S_a [6].

The calculated roughness values S_a and S_q are plotted for each matrix (corresponding to a fixed pulse energy) against the pulse-to-pulse translation distance and the repetition frequency; subsequently a second-order polynomial is fitted to the data corresponding to each matrix. The fit quality for the roughness data of an entire matrix is lower than the fit quality for the depth data and does not allow to identify a clear trend of roughness as a function of pulse-to-pulse translation distance and laser repetition frequency. A better fit is obtained considering separately different surface textures; considering for example only the pockets which belong to the “no debris” category a better second-order polynomial fit is reached.

Figure 10 shows the fit for S_a (e.g.) for the “no debris” pockets for 100% pulse energy. We compare this fit to the fit we obtained considering together the pockets belonging to the “no debris” and “debris” categories (Figure 11); the fit for both categories together is relatively good, but not as good as the one obtained considering only the “no debris” pockets. This is an indication that thermal effects may have an influence on the surface roughness.

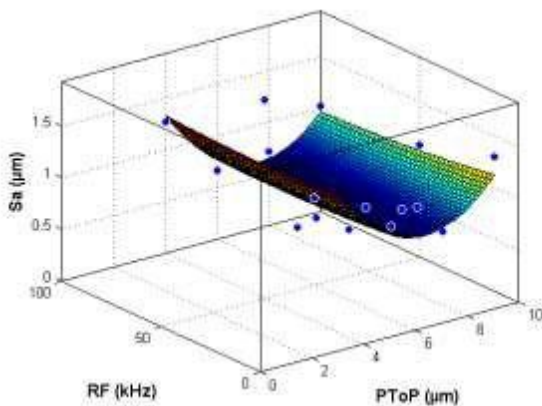


Figure 10: Roughness S_a of the pockets machined with 100% pulse energy plotted against pulse-to-pulse translation distance (μm) and repetition frequency (kHz) and corresponding best-fitting function

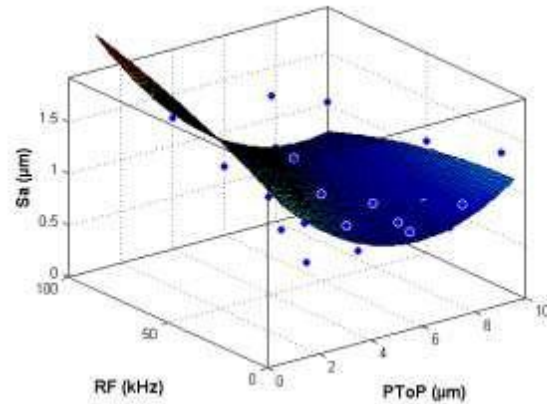


Figure 11: Roughness S_a of the pockets machined with 100% pulse energy plotted against pulse-to-pulse translation distance (μm) and repetition frequency (kHz) and corresponding best-fitting function

For a more detailed view of the data we plot in Figure 12 the roughness value S_a against the pulse-to-pulse translation distance for fixed repetition frequency; the green dots represent pockets belonging to the “no debris” category, and blue dots pockets belonging to the “debris” category. The roughness value S_a reaches a minimum between pulse-to-pulse translation distances of 8 and 10 μm , a value approximately corresponding to the beam waist radius ($w_0 = 9.4 \mu\text{m}$). A similar trend is shown for polyimide in a paper by B. Pratap and co-authors [7].

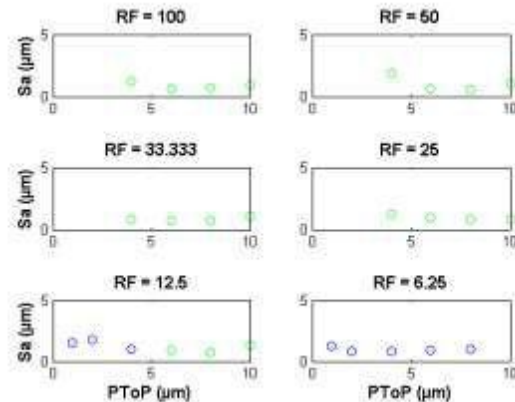


Figure 12: Roughness parameter S_a (μm) against the pulse-to-pulse translation distance (μm) for fixed repetition rate at 100% pulse energy; the green dots represent pockets of the “no debris” category and the blue ones of the “debris” category.

Analysis of the multi-pass machining experiment

For the multi-pass experiment five selected pockets are examined. All of these pockets are chosen in the “no debris” or “debris” regions; the machining parameters for the selected pockets are listed in Table 2. A plot of depth against number of passes is done for each selected set of machining parameters; Figure 13 shows the plot obtained for the parameter set of 100% pulse energy, pulse-to-pulse translation distance of 4 μm and repetition frequency of 25 kHz. An examination of the plot shows that the depth increases linearly with the number of passes; this behavior occurs for all of the selected parameter sets.

The roughness value is also plotted against the number of passes in Figure 14; again, the green dots correspond to the “no debris” case and the blue ones the “debris” case. In this case no trend common to all of the parameter sets is easily discernible; despite the lack of a general trend in the dependence of the roughness on the number of passes, multi-pass machining can still improve the control one has on the roughness. We will discuss how in the following section.

Discussion and conclusions

A good insight in the experimental data can be obtained with the help of contour plots of the best-fit functions to the depth and roughness datasets seen as functions of the pulse-to-pulse translation distance and laser repetition frequency. Figure 15 shows the contour plot of the depth fit function and Figure 16 likewise shows the contour plot for the roughness value best-fit function; each of them for the dataset corresponding to the matrix of pockets machined with a single-pass at 100% pulse energy. In the contour plot in Figure 15 it is apparent that the ablation depth stays approximately constant for a fixed pulse-to-pulse translation distance. Increasing the repetition rate allows faster machining (a higher ablation rate); one needs to consider as a possible limit the onset of thermal effects.

A comparison of the contour plot for the depth with the contour plot for the roughness shows that the contour lines in the two graphs are approximately parallel to each other; this means that, if one is limited to single-pass machining, it is not possible to choose independently the depth and the roughness of a pocket.

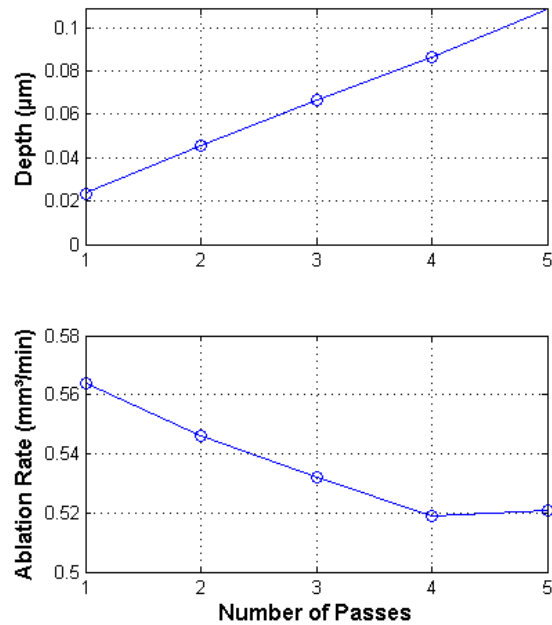


Figure 13: Depth of the ablated pocket against the number of passes in the multi-pass experiment. The machining parameters for each pass are listed in row 1 of Table 2

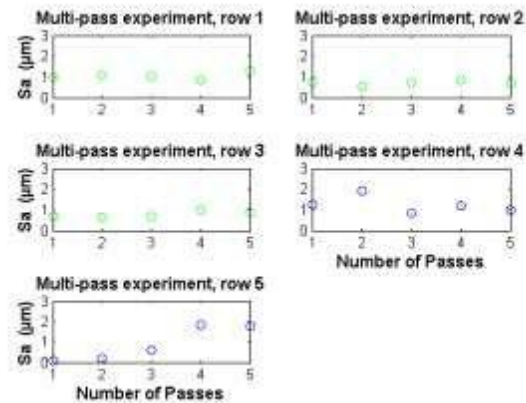


Figure 14: Roughness parameter Sa for plotted against the number of passes for the multi-pass experiment; the machining parameters for each row of pockets are listed in Table 2

Multiple-pass machining allows more flexibility – despite the fact that the trend roughness versus number of passes is not uniform for all machining parameters. Taking a look for example at row 1, we see that the roughness stays approximately constant while the ablation depth increases; roughness and ablation depth become in this way somewhat independent from each other. By selecting in an appropriate way machining parameters together with number of passes it is possible to achieve different roughness characteristics for a given depth.

Table of content

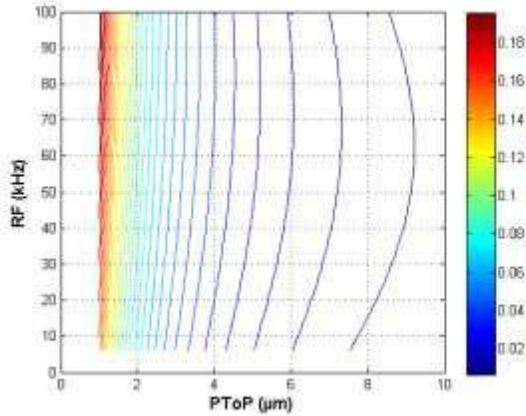


Figure 15: Contour plot for the depth (mm) as a function of pulse-to-pulse translation distance (μm) and laser repetition frequency (kHz); data relative to 100% pulse energy

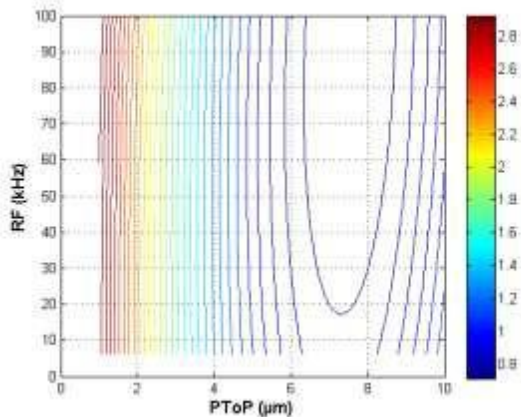


Figure 16: Contour plot for the roughness parameter S_a (μm) as a function of pulse-to-pulse translation distance (μm) and laser repetition frequency (kHz); data relative to 100% pulse energy

In conclusion we performed a systematic study of ablation depth and roughness for an extended set of ultrashort-pulse laser machining parameters. We classified qualitatively surface textures obtained by machining parameters in a way that is related to thermal stress and we verified that, for the machining conditions and strategy we investigated, if single-pass machining is used the ablation depth and the surface roughness are tied to each other, while multiple-pass machining allows a certain degree of freedom in selecting independently depth and roughness.

- [1] M. Stöver and E. Wintermantel, "Oberflächenstrukturierung metallischer Werkstoffe, z. B. für stents," in *Medizintechnik*. Berlin Heidelberg: Springer Verlag, 2009, pp. 943-949.
- [2] R. Ortiz et al., "Ultra-fast laser microprocessing of medical polymers for cell engineering applications," in *Materials Science and Engineering: C*. Amsterdam: Elsevier Verlag, 2014, pp. 241-250.
- [3] S. Labisch and C. Weber, *Technisches Zeichnen*, 4th ed., Springer Fachmedien, Ed. Wisbaden: Springer Fachmedien, 2014.
- [4] P. R. Miller et al., "Laser Micromachining for Biomedical Applications," *JOM*, vol. 61, no. 9, pp. 35-40, 2009.
- [5] R. Truckenmüller et al., "Fabrication of cell container arrays with overlaid surface topographies," *Biomedical Microdevices*, pp. 95-107, Feb. 2012.
- [6] S. Jung, "Oberflächenbeurteilung," Uni Stuttgart, Stuttgart, Lecture notes n.y. [Online]. <http://goo.gl/BPqicA>
- [7] B. Pratap, C. B. Arnold, and A. Piqué, "Depth And Surface Roughness Control On Laser Micromachined Polyimide For Direct-Write Deposition," *SPIE MF 2003*, vol. 4979, pp. 217-226, Jan. 2003.